

Measurements of the lower critical field of superconductors using NV centers in diamond optical magnetometry

K. R. Joshi,^{1,2} N. M. Nusran,¹ K. Cho,¹ M. A. Tanatar,^{1,2}
W. R. Meier,^{1,2} S. L. Bud'ko,^{1,2} P. C. Canfield,^{1,2} and R. Prozorov^{1,2,*}

¹Ames Laboratory, Ames, IA 50011

²Department of Physics & Astronomy, Iowa State University, Ames, IA 50011

(Dated: 27 June 2018)

The lower critical magnetic field, H_{c1} , of superconductors is measured by using ensembles of NV-centers-in-diamond optical magnetometry. The technique is minimally invasive, and has sub-gauss field sensitivity and sub- μm spatial resolution, which allow for accurate detection of the vector field at which the vortices start penetrating the sample from the corners. Aided by the revised calculations of the effective demagnetization factors of actual cuboid - shaped samples, H_{c1} and the London penetration depth, λ , derived from H_{c1} can be obtained. We apply this method to three well-studied superconductors: optimally doped $\text{Ba}(\text{Fe}_{1-x}\text{Co}_x)_2\text{As}_2$, stoichiometric $\text{CaKFe}_4\text{As}_4$, and high- T_c cuprate $\text{YBa}_2\text{Cu}_3\text{O}_{7-\delta}$. Our results are well compared with the values of λ obtained using other techniques, thus adding another non-destructive and sensitive method to measure these important parameters of superconductors.

I. INTRODUCTION

A. Lower critical magnetic field

The lower (first) critical field, H_{c1} , is one of the important fundamental parameters characterizing any type-II superconductor [1]. Above this field, Abrikosov vortices become energetically favorable and start entering the sample from the edges. Importantly, H_{c1} is related to two fundamental length scales: the London penetration depth, λ , and the coherence length ξ , as follows, [2]

$$H_{c1} = \frac{\phi_0}{4\pi\lambda^2} \left(\ln \frac{\lambda}{\xi} + 0.497 \right) \quad (1)$$

ξ enters Eq.(1) only under the logarithm and there are other more direct/sensitive ways to determine it experimentally (for example from the upper critical field, $H_{c2} = \phi_0 / (2\pi\xi^2)$, where $\phi_0 = 2.07 \times 10^{-15}$ Wb is magnetic flux quantum. Thus, the London penetration depth λ is often estimated using Eq.(1) if H_{c1} is experimentally given. In terms of the numerical values, for example, for studied here $\text{Ba}(\text{Fe}_{1-x}\text{Co}_x)_2\text{As}_2$ (122) iron-based superconductors [3, 4], $\xi \approx 2.3$ nm, $\lambda \approx 200$ nm, so that $\kappa = \lambda/\xi \approx 87$, which give $H_{c1} \approx 200$ Oe and $H_{c2} \approx 60$ T. For optimally - doped $\text{YBa}_2\text{Cu}_3\text{O}_{7-\delta}$ (YBCO) [5–7], $\xi \approx 1.6$ nm, $\lambda \approx 140 - 160$ nm, $\kappa \approx 80 - 100$, $H_{c1} \approx 350 - 400$ Oe and $H_{c2} \approx 120$ T.

In practice, using Eq.(1) to determine H_{c1} has two major difficulties: (1) the existence of various surface barriers [8–10] that inhibit the penetration of a magnetic field, hence lead to over-estimation of H_{c1} , and (2) the distortion of a magnetic field around an actual, finite size sample that leads to under-estimation of H_{c1} . Therefore, the

experimentally detected onset of the magnetic field penetration, denoted here H_p , coincides with H_{c1} only in case of an infinite slab in a parallel magnetic field and no surface barrier, a configuration which is almost impossible to achieve in experiment. However, analysis shows that H_p is directly proportional to H_{c1} with the appropriate geometric conversion factor [10, 11]. Several previous works analyzed the situation and now most experimentalists follow the numerical results published by E. H. Brandt who used approximate nonlinear $E(j)$ characteristics to estimate the connection between H_p and H_{c1} [10, 11].

Here, it is important to understand how H_p is defined. The E. H. Brandt's picture of the magnetic flux penetration into the samples with rectangular cross-sections, known as the “geometric barrier”, is illustrated Fig. 1. In the normal state (top left panel of Fig. 1) magnetic field fills nonmagnetic sample uniformly. In the superconducting Meissner state, weak magnetic field is (almost) completely shielded from the interior (top right panel of Fig. 1), except for the very small layer of London penetration depth, invisible in Fig. 1. Upon further increase, when maximum local magnetic field $H/(1-N)$, becomes equal to the lower critical field, H_{c1} , Abrikosov vortices nucleate and start penetrating the sample. In the present case of a rectangular prism, the maximum field is reached at the corners and straight vortex segments start entering the sample at approximately 45 degrees (bottom left panel of Fig. 1) [11]. Since vortex segment length increases, its free energy increases as a function of position from the edge. This is equivalent to a repulsive force that is preventing such vortex from entering the sample. This is the mechanism of a “geometric barrier” [10, 11], which is very different from a Bean-Livingston surface barrier that requires straight smooth surfaces that attract just formed straight vortex lines to their images [8]. When top and bottom segments meet in the middle of the side (at the “equator”, bottom right panel of Fig. 1) continuous vortex lines are formed. Without pinning, they will im-

* Corresponding author: prozorov@ameslab.gov

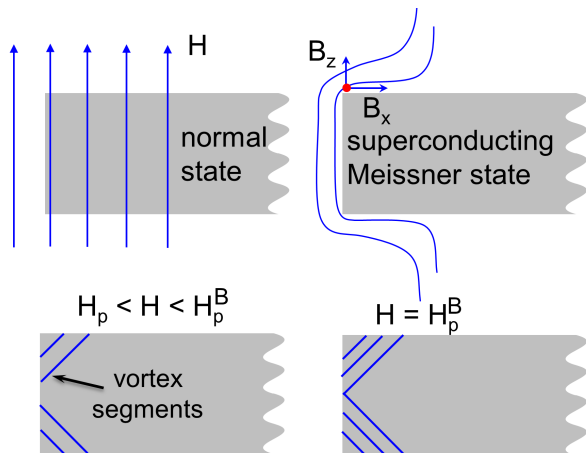


FIG. 1. Schematics of the magnetic field penetration into a rectangular cross-section sample (only sample side is shown). Top left: normal state. Top right: genuine Meissner state with no vortices and only London penetration depth layer is filled with a magnetic field. Lower left: at $H_p = (1 - N)H_{c1}$, Abrikosov vortices start entering the sample from the corners at an angle approximately 45° [10, 11]. Lower right: at $H = H_p^B$ vortex segments meet in the middle of the edge forming a continuous vortex line. Without pinning, these vortices will be immediately moved by the Lorentz force to the sample center.

mediately be pushed to the sample center by the Lorentz force from the currents due to vortex density gradient. At this value of the applied field, which we denote as H_p^B (“B” emphasizes that this is Brandt’s definition [11]), the magnetization, $M(H)$, reaches a maximum amplitude and $H_p^B \approx H_{c1} \tanh \sqrt{\alpha c/a}$, where $\alpha = 0.36$ for an infinite (in the b -direction) strip or $\alpha = 0.67$ for disks of radius a [10, 11]. Note that at this field, H_p^B , a significant volume of the sample around its perimeter is already occupied by vortices (from the corner segment penetration) and a local magnetic field at the corners has far exceeded H_{c1} . In fact this the described scenario is the essence of so-called geometric barrier [11]. (With pinning, above H_p^B , vortices will fill the interior according to the critical state model and the $M(H)$ curve will become more non-linear, but will not attain the maximum value until vortices reach sample center.)

An alternative definition of H_p is based on the deviation of local magnetic induction from zero or total magnetic moment from linear $M(H)$ behavior. In practice, the local magnetic induction, B , is measured outside the sample, on its surface close to the sample edge. The external magnetic field expelled by the sample leaks into the sensor, so that measured $B(H)$ is always non zero, but is still linear in H and it deviates from linearity when vortices start to penetrate the sample from the corners and this can be detected as the the onset of flux penetration field H_p [12, 13]. Similar estimate can be obtained from the $M(H)$ curves detecting the deviation from linear behavior upon application of a magnetic field after cooling in zero field [14]. Another version of this approach

is to look for the remnant flux trapped inside the superconductor which becomes non-zero when a lower critical field is reached in any part of the sample, vortices penetrated and became trapped due to ubiquitous pinnings [15]. In all these scenarios, the lower critical field should be obtained with the appropriate effective demagnetization factor, N ,

$$H_p = H_{c1} (1 + N\chi) \quad (2)$$

where χ is the “intrinsic” magnetic susceptibility of the material (i.e., in an “ideal” sample with no demagnetization and surface barriers), which can be taken to be equal to -1 for a robust superconductor at most temperatures below T_c (for an infinite slab of width $2w$ in a parallel field, $\chi = \lambda/w \tanh(w/\lambda) - 1$ and it is straightforward to check that χ is still less than -0.995 even at $T/T_c = 0.99$).

Unfortunately, most previous works that employed local measurements of the onset of magnetic flux penetration using, for example, miniature Hall probes [12, 13, 15], analyzed the data with Brandt’s formulas for H_p^B and not with the (more correct in this case) H_p from Eq.(2).

B. Effective demagnetizing factors

To use H_p for determining H_{c1} , the effective demagnetizing factor, N , has to be calculated for specific sample geometry. Indeed, strictly speaking, N is only defined for ellipsoidal samples, which is of little practical use for typical samples of a cuboidal (rectangular prism) shape. Yet, it is possible to introduce effective demagnetizing factors which were calculated in several previous works, including the cited Brandt’s papers, since his estimate of H_p^B implicitly includes the effective N [11]. As we recently showed from a full 3D finite-element analysis [16], Brandt provided very accurate expressions for demagnetizing factors in cases of infinite strips or disks of rectangular cross-section, see Eq.(7) in Ref.[11]. However, we also found that the effective demagnetizing factors for finite cuboids are quite different from the infinite 2D strips and, therefore, the whole methodology of estimating H_{c1} from magnetic measurements should be revisited. This is the subject of the present work.

Although we can calculate the effective demagnetization factor with arbitrary precision for a sample of any shape, it is always useful to have simple, but accurate enough formulas [16]. A good approximation for a $2a \times 2b \times 2c$ cuboid in a magnetic field along the c -direction is given by [16],

$$N^{-1} = 1 + \frac{3c}{4a} \left(1 + \frac{a}{b}\right) \quad (3)$$

Having samples of rectangular cross-section is problematic from the uncertainty in demagnetization effects point of view, but it is advantageous in terms of the (absence) of surface barriers, because now magnetic flux

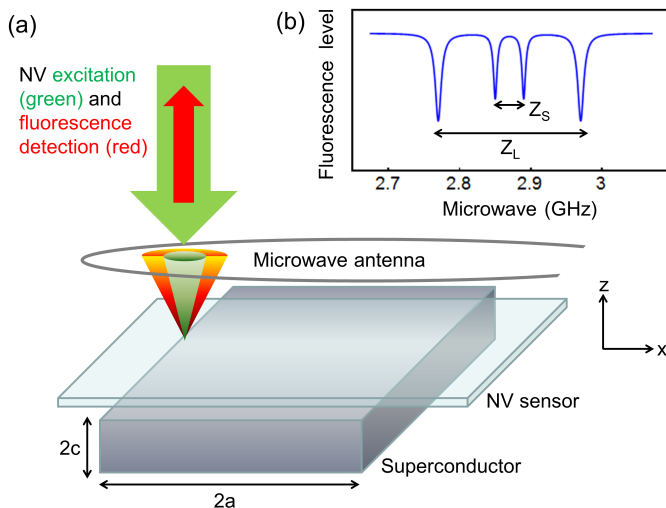


FIG. 2. (a) Schematics of the key components of the NV sensing setup (b) Optically detected magnetic resonance (ODMR) spectrum for local magnetic field vector with two components, $\vec{B} = (B_x, 0, B_z)$. (See text for details.)

penetrates from the corners and not parallel to the extended flat surfaces which is how surface barriers are formed [8]. Moreover, the “geometric barrier” that essentially involves the flux corner penetration described above [10, 11] is not relevant if the onset of nonlinearity is detected near the sample edge.

II. EXPERIMENTAL

A. Optical magnetic sensing using NV centers in diamond

In this work, the vector magnetic induction on the sample surface was measured using optical magnetometry based on nitrogen-vacancy (NV) color centers in diamond. Specifically, the optically detected magnetic resonance (ODMR) of Zeeman split energy levels in NV centers, proportional to a local magnetic field, is measured [17]. The NV-centers’ magneto-sensing has several important advantages for measurements of delicate effects in superconductors. (1) It is minimally invasive, - the magnetic moment of the probe itself is of the order of a few Bohr magnetons, μ_B , and hence has negligible effect on the measured magnetic fields. (2) It has sufficient spatial resolution, - sub-micrometer spatial mapping can be achieved even with the ensemble mode of NV sensing. (3) It is capable to measure a vector magnetic induction [18]. This is particularly important as the detection of flux penetration depends on the location, and magnetic field lines deviate significantly from the direction of the applied field [16].

Measurement protocols, experimental schematics and deconvolution of the ODMR spectrum into magnetic field

components are discussed in detail in our previous work in which the spatial structure of the Meissner state in various superconductors was studied [18]. Here, we focus particularly on the measurements of the lower critical field, H_{c1} , and summarize the key experimental details for completeness.

To measure a local magnetic induction, a magneto-optical “indicator” ($1.5 \times 1 \times 0.04 \text{ mm}^3$ diamond plate with embedded NV centers) is placed on top of the superconducting sample with its NV-active side facing the sample surface. On the “active” side, NV centers are created within $\sim 20 \text{ nm}$ from the surface of a single crystalline diamond plate using commercial protocols that involve nitrogen ion implantation, electron irradiation and high temperature annealing in high vacuum. The diamond plate has (100) crystal surface and [100] edges. Therefore, NV centers are oriented along all four [111] diamond axes, which define the directions of the magnetic field sensing. As a result, possible Zeeman splittings in a random ensemble of NV centers in (indeed, a single crystal of) diamond is given by $2\gamma_e|\vec{B} \cdot \hat{d}|$, where $\gamma_e \approx 2.8 \text{ MHz/G}$ is the gyromagnetic ratio of the NV-center electronic spin, and \hat{d} is a unit vector along any of the four diamond axes. In a magnetic field along the \hat{z} direction, i.e., $\vec{B} = (0, 0, B_z)$, all possible NV orientations result in the same splitting,

$$Z = \frac{2\gamma_e B_z}{\sqrt{3}} \approx 3.233 \text{ MHz/G}$$

whereas, if the magnetic field has two components such that $\vec{B} = (B_x, 0, B_z)$, the NV ensemble will result in two pairs of Zeeman splittings:

$$Z_{L,S} = Z|B_z \pm B_x|$$

where, Z_L (Z_S) refers to larger (smaller) Zeeman splitting. An example of such two-pairs of ODMR splitting spectrum is shown in Fig.2(b).

B. Experimental setup and samples

The experimental setup is based on the Attocube CFM/AFM system and includes a confocal microscope optimized for the NV fluorescence detection inside the helium cryostat with optical parts in vacuum and the sample placed on a temperature-controlled cold stage. A schematic of the experiment is shown in Fig.2(a). The objective is focused on the NV centers in a (optically transparent) diamond plate, so that the convolution of the diffraction limited confocal volume with the NV distribution leads to essentially a disk shaped sensing volume of thickness $\approx 20 \text{ nm}$ and diameter $\approx 500 \text{ nm}$. The diamond plate is placed directly on top of a flat sample surface covering the edge and with NV active side facing the sample. A $50\times$ confocal microscope objective is used both for green laser excitation and red fluorescence

collection. Microwave radiation with a very small amplitude is applied using a single-turn $50\ \mu\text{m}$ diameter silver wire.

All samples were pre-characterized using various thermodynamic and transport techniques (see, e.g., Ref. [19]) and imaged using scanning electron microscopy (SEM) and only samples with well-defined surfaces and edges, as shown in Fig.3(a), were selected for further measurements.

III. MEASUREMENTS OF THE LOWER CRITICAL FIELD

The experimental protocol for measurements of H_{c1} is as follows:

(1) The sample is cooled to the target temperature below T_c in the absence of a magnetic field (zero-field cooling, ZFC). Then, a small magnetic field (10 Oe in our case, much smaller than 200 - 400 Oe expected for H_{c1} at low temperatures as discussed in the introduction) is applied and ODMR signals are recorded at different points along the line perpendicular to the sample edge. Measured ODMR splittings are then converted into the magnetic induction values as described above. This, combined with direct visualization of the sample through a transparent diamond plate, allows for accurate determination of the location of the sample edge and provides information about sample homogeneity. The quality of the superconductor is also verified by looking at the sharpness of the transition detected by the ODMR splitting recorded as a function of temperature at any fixed point over the sample, see, e.g., Fig.3(b).

(2) After this initial preparation and edge identification, the magnetic field is removed, the sample is warmed up to above T_c and then cooled back down to a target temperature, thereby resetting it to the genuine superconducting state with no trapped magnetic field inside. A point inside and over the sample, but close to the edge, is chosen and ODMR spectra are recorded as a function of external magnetic field, which is applied incrementally in small steps. At each step, the superconducting magnet is switched to a persistent mode to insure stability of the magnetic field. The deviation from the linear behavior in Z_S is then detected and recorded as the field of first flux penetration, H_p .

(3) Now, using Eq.(2), (3), and (1), the value of H_{c1} and the London penetration depth λ are evaluated. This procedure is repeated at several locations along the edge to ensure objectivity of the result.

IV. RESULTS AND DISCUSSION

To illustrate the described method, we measured H_{c1} and evaluated the London penetration depth, λ , in three different superconducting materials.

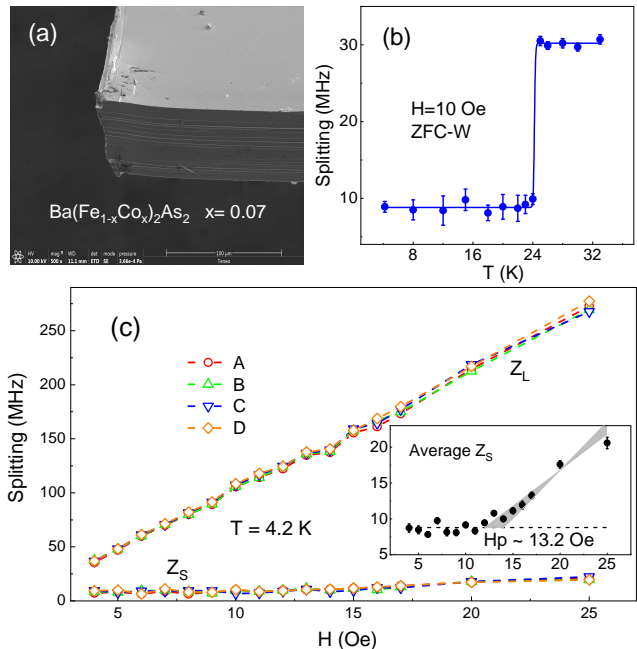


FIG. 3. (a) Scanning electron microscope (SEM) image of the measured single crystal of $\text{Ba}(\text{Fe}_{1-x}\text{Co}_x)_2\text{As}_2$, $x=0.07$ (b) Detection of superconducting phase transition at $T_c \approx 24\ \text{K}$ (c) H_{c1} measurements of this sample at 4.2 K. Zeeman splittings measured at four different points, A, B, C and D near the edge as a function of the increasing magnetic field applied after ZFC. Inset shows a clear change at $H_p=13.2\pm 1\ \text{Oe}$ of the 4-point-averaged signal of the Z_S

A. $\text{Ba}(\text{Fe}_{1-x}\text{Co}_x)_2\text{As}_2$, $x = 0.07$

A well characterized optimally doped single crystal of $\text{Ba}(\text{Fe}_{1-x}\text{Co}_x)_2\text{As}_2$, $x = 0.07$ (FeCo122) of cuboidal shape with dimensions, $1.0 \times 1.2 \times 0.05\ \text{mm}^3$, was selected. An SEM image in Fig.3(a) shows a well-defined prismatic corner with flat clean surface and straight edges. The superconducting transition temperature, $T_c \approx 24\ \text{K}$, determined from a conventional magnetometer, was also consistent with our ODMR measurements at the location on the sample surface inside the sample as shown in Fig.3(b). ODMR splittings at four different locations on the sample surface near the edge are labeled A, B, C, and D in Fig.3(c). These four points are approximately $5\ \mu\text{m}$ far apart from neighbor points and each point is approximately $10\ \mu\text{m}$ from the edge inside the sample. As discussed above, the two Zeeman splittings Z_L and Z_S correspond to linear combinations of horizontal (B_x) and vertical (B_z) components of the magnetic induction as described above. Notice excellent reproducibility of the results indicating homogeneous superconducting properties of our sample. The inset Fig.3(c) shows average (of four points) small splitting signal (Z_S). A clear onset of first flux penetration is determined at at $H_p=13.2\pm 1\ \text{Oe}$.

To understand the observed ODMR splittings, we con-

sider Brandt's results of flux corner cutting and entering in form of Abrikosov vortices approximately at an angle of 45° with respect to the corner. Therefore the normal to the sample surface z -component (along the applied field) and longitudinal, x -component of the magnetic induction are approximately equal and proportional to the applied field. This linear relation continues with the increasing applied field until a critical value of the first flux penetration field, H_p , is reached. At this point, angle of the magnetic flux at the sample edges deviates from 45° trending more towards \hat{z} direction. This scenario can be phenomenologically modeled by representing the magnetic induction components as: $B_{z,x} = DH \pm \delta$ and $\delta = 0 + \alpha\theta(H - H_p)(H - H_p)^n$ where D is an effective demagnetization factor and $\theta(H)$ is a Heaviside step function. Because the larger splitting $-Z_L$ and smaller splitting $-Z_S$ are proportional to the sum and difference of $B_{z,x}$ components respectively, the change at H_p is reflected clearly in Z_S but not in Z_L . The Zeeman splittings observed in Fig.3(c) can be understood with this model for the parameters: $D = 3.5$, $H_p = 13.2$, $\alpha = 0.6$, and $n = 1$. Hence, this provides an experimental confirmation for Brandt's description of flux corner cutting and entering approximately at an angle of 45° with respect to its sides.

From the experimental value of H_p and effective demagnetization factor for this particular sample, $N = 0.9168$ we obtain using Eq.(2), $H_{c1} = 158 \pm 12$ Oe. And with the use of Eq.(1) and taking $\xi \approx 2.3$ nm, we obtain the final result, $\lambda = 226 \pm 10$ nm. This estimate for London penetration depth is comparable with the values obtained from other techniques such as μ SR - 224 nm [20] and MFM - 245 nm [21]. The agreement is quite good and gives confidence in the validity of the developed technique. Table (I) summarize all these estimates. The estimates obtained using Brandt's formula for an infinite rectangular strip are also given for comparison.

B. $\text{CaKFe}_4\text{As}_4$

The cuboid - shaped single crystal of stoichiometric $\text{CaKFe}_4\text{As}_4$ with dimensions of $1.01 \times 0.99 \times 0.01$ mm³ was studied. The inset in Fig.4(a) shows a sharp superconducting phase transition at $T_c \approx 34$ K. The average of ODMR splitting, Z_S , near the sample edge as a function of the applied magnetic field clearly shows a break associated with the magnetic flux penetration at $H_p = 8.3 \pm 1.1$ Oe. The error here is determined visually by the shaded region which spans all measurement points. Using Eq.(2) and (3), this results in the estimation of $H_{c1} = 394 \pm 52$ Oe. Now, using Eq.(1) and $\xi \approx 2.15$ nm [19], we estimate $\lambda = 141 \pm 11$ nm. This result was used to calculate the superfluid density in Ref.[19], which was consistent with isotropic two-gap s_{\pm} pairing state.

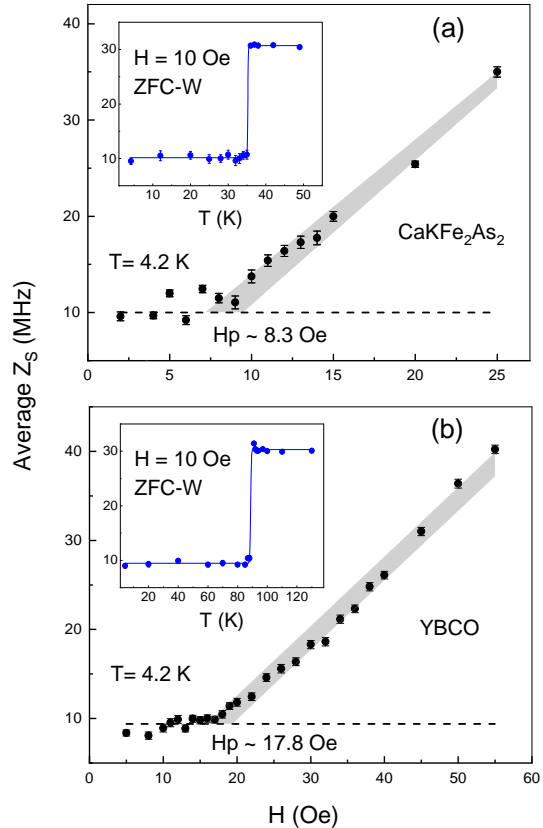


FIG. 4. Measurements of the field of first flux penetration, H_p , in single crystals of (a) $\text{CaKFe}_4\text{As}_4$ and (b) $\text{YBa}_2\text{Cu}_3\text{O}_{7-\delta}$. Insets show superconducting phase transitions at $T_c \approx 34$ K and 88 K, respectively.

C. $\text{YBa}_2\text{Cu}_3\text{O}_{7-\delta}$

To look at a very different system, we also measured a single crystal of a well known cuprate superconductor, $\text{YBa}_2\text{Cu}_3\text{O}_{7-\delta}$ (YBCO). The sample dimensions were $0.5 \times 0.85 \times 0.017$ mm³. The inset in Fig.4(b) shows a sharp superconducting phase transition at $T_c \approx 88$ K. The clear break associated with the magnetic field of first flux penetration in the average Z_S vs H plot is observed at $H_p = 17.8 \pm 1.6$ Oe. Using Eq.(2) and (3), this leads to estimation of $H_{c1} = 344 \pm 31$ Oe. Using Eq.(1) and coherence length $\xi \approx 1.6$ nm [5, 7], we estimate $\lambda \approx 156 \pm 8$ nm. All estimates including values obtained using Brandt's formula for a rectangular strip and from other techniques are summarized in Table (I). Once again a good agreement is seen between our estimates and the values reported in the literature obtained from other techniques such as μ SR - 155 nm [25], microwave cavity perturbation technique, 160 nm [24] and tunnel-diode resonator, 140 nm [6].

Superconductor	T_c (K)	H_{c1}^{2D} (G)	λ_{ab}^B (nm)	H_{c1} (G)	λ_{ab} (nm)	λ (nm) (literature)
FeCo122	24.3	102±8	288±12	158±12	226±10	270,245,224 [20–22]
CaKFe ₄ As ₄	34	139±18	251±18	394±52	141±11	208,187 [23]
YBCO	88.3	163±15	236±12	344±31	156±8	146,160,155,149 [6, 24–26]

TABLE I. Estimates for H_{c1} and λ_{ab} . Here λ_{ab}^B is calculated using Brandt’s formula for H_p^B in an infinite strip.

V. CONCLUSIONS

To summarize, we used NV-centers in diamond for optical vector magnetic field sensing at low temperatures to measure the lower critical field, H_{c1} , in type II superconductors. The minimally-invasive nature and optical diffraction-limited small size of the probe makes NV sensor ideal for this purpose. The capability of resolving vector components provides a unique advantage, which allowed direct verification of the E. H. Brandt’s model of magnetic flux penetration that proceeds via corner cutting by vortices at a $\approx 45^\circ$ angle with respect to the edges. We applied this technique to three different superconductors: optimally doped FeCo122, stoichiometric CaKFe₄As₄, and high- T_c cuprate, YBCO. London penetration depth values evaluated from the obtained H_{c1} are

in a good agreement with the literature with the largest uncertainty for CaK1144, most likely due to various levels of scattering in samples studied in different works. Our approach is very useful non-destructive way to estimate $\lambda(0)$ that is needed to obtain superfluid density, which is the quantity that can be compared with theory.

ACKNOWLEDGEMENT

This work was supported by the U.S. Department of Energy (DOE), Office of Science, Basic Energy Sciences, Materials Science and Engineering Division. The research was performed at Ames Laboratory, which is operated for the U.S. DOE by Iowa State University under contract # DE-AC02-07CH11358. W. M. was supported by the Gordon and Betty Moore Foundation’s EPIQS Initiative through Grant GBMF4411.

-
- [1] M. Tinkham, *Introduction to Superconductivity*, 2nd ed., Dover Books on Physics (2004).
 - [2] Chia-Ren Hu, “Numerical constants for isolated vortices in superconductors,” *Phys. Rev. B* **6**, 1756–1760 (1972).
 - [3] Paul C. Canfield and Sergey L. Bud’ko, “FeAs-Based Superconductivity: A Case Study of the Effects of Transition Metal Doping on BaFe₂As₂,” *Ann. Rev. Cond. Mat. Phys.* **1**, 27–50 (2010).
 - [4] R. Prozorov and V. G. Kogan, “London penetration depth in iron-based superconductors,” *Rep. Prog. Phys.* **74**, 124505 (2011).
 - [5] K. E. Gray, D. H. Kim, B. W. Veal, G. T. Seidler, T. F. Rosenbaum, and D. E. Farrell, “High anisotropy and a dimensionality crossover in the irreversibility behavior of oxygen-deficient YBaCuO,” *Phys. Rev. B* **45**, 10071–10074 (1992).
 - [6] R. Prozorov, R. W. Giannetta, A. Carrington, P. Fournier, R. L. Greene, P. Guptasarma, D. G. Hinks, and A. R. Banks, “Measurements of the absolute value of the penetration depth in high- T_c superconductors using a low- T_c superconductive coating,” *Appl. Phys. Lett.* **77**, 4202–4204 (2000).
 - [7] T. Sekitani, N. Miura, S. Ikeda, Y. H. Matsuda, and Y. Shiohara, “Upper critical field for optimally-doped YBa₂Cu₃O_{7- δ} ,” *Physica B* **346-347**, 319 – 324 (2004).
 - [8] C. P. Bean and J. D. Livingston, “Surface Barrier in Type-II Superconductors,” *Phys. Rev. Lett.* **12**, 14–16 (1964).
 - [9] E H Brandt, “The flux-line lattice in superconductors,” *Rep. Prog. Phys.* **58**, 1465–1594 (1995).
 - [10] Ernst Helmut Brandt, “Geometric barrier and current string in type-II superconductors obtained from continuum electrodynamics,” *Phys. Rev. B* **59**, 3369–3372 (1999).
 - [11] E. H. Brandt, “Geometric edge barrier in the Shubnikov phase of type-II superconductors,” *Low Temp. Phys.* **27**, 723–731 (2001).
 - [12] Ryuji Okazaki, Marcin Konczykowski, Cornelis van der Beek, Terukazu Kato, Kenichiro Hashimoto, M Shimozawa, H Shishido, Minoru Yamashita, Motoyuki Ishikado, Hijiri Kito, Akira Iyo, Hiroshi Eisaki, Shinichi Shamoto, Takasada Shibauchi, and Yuji Matsuda, “Lower critical fields of superconducting PrFeAsO single crystals,” *Phys. Rev. B* **79**, 064520 (2009).
 - [13] T. Klein, D. Braithwaite, A. Demuer, W. Knafo, G. Lapertot, C. Marcenat, P. Rodière, I. Sheikin, P. Strobel, A. Sulpice, and P. Toulemonde, “Thermodynamic phase diagram of Fe(Se_{0.5}Te_{0.5}) single crystals in fields up to 28 tesla,” *Phys. Rev. B* **82**, 184506 (2010).
 - [14] M. Abdel-Hafiez, J. Ge, A. N. Vasiliev, D. A. Chareev, J. Van de Vondel, V. V. Moshchalkov, and A. V. Silhanek, “Temperature dependence of lower critical field $H_{c1}(t)$ shows nodeless superconductivity in FeSe,” *Phys. Rev. B* **88**, 174512 (2013).
 - [15] Z. Pribulova, T. Klein, J. Kacmarcik, C. Marcenat, M. Konczykowski, S. L. Bud’ko, M. Tillman, and P. C. Canfield, “Upper and lower critical magnetic fields of superconducting ndfeasof single crystals studied by hall-probe magnetization and specific heat,” *Phys. Rev. B* **79**, 020508 (2009).

- [16] R. Prozorov and V. G. Kogan, “Effective demagnetization factors of diamagnetic samples of various shapes,” arXiv:1712.06037 (2018).
- [17] L. Rondin, J. P. Tetienne, S. Rohart, A. Thiaville, T. Hingant, P. Spinicelli, J. F. Roch, and V. Jacques, “Stray-field imaging of magnetic vortices with a single diamond spin,” *Nat. Commun.* **4**, 2279 (2013).
- [18] N M Nusran, K R Joshi, K Cho, M A Tanatar, W R Meier, S L Budko, P C Canfield, Y Liu, T A Lograsso, and R Prozorov, “Spatially-resolved study of the meissner effect in superconductors using nv-centers-in-diamond optical magnetometry,” *New J. Phys.* **20**, 043010 (2018).
- [19] Kyuil Cho, A. Fente, S. Teknowijoyo, M. A. Tanatar, K. R. Joshi, N. M. Nusran, T. Kong, W. R. Meier, U. Kaluarachchi, I. Guillamón, H. Suderow, S. L. Bud’ko, P. C. Canfield, and R. Prozorov, “Nodeless multiband superconductivity in stoichiometric single-crystalline $\text{CaKFe}_4\text{As}_4$,” *Phys. Rev. B* **95**, 100502 (2017).
- [20] T. J. Williams, A. A. Aczel, E. Baggio-Saitovitch, S. L. Bud’ko, P. C. Canfield, J. P. Carlo, T. Goko, H. Kageyama, A. Kitada, J. Munevar, N. Ni, S. R. Saha, K. Kirschenbaum, J. Paglione, D. R. Sanchez-Candela, Y. J. Uemura, and G. M. Luke, “Superfluid density and field-induced magnetism in $\text{Ba}(\text{Fe}_{1-x}\text{Co}_x)_2\text{As}_2$ and $\text{Sr}(\text{Fe}_{1-x}\text{Co}_x)_2\text{As}_2$ measured with muon spin relaxation,” *Phys. Rev. B* **82**, 094512 (2010).
- [21] Lan Luan, Thomas M. Lippman, Clifford W. Hicks, Julie A. Bert, Ophir M. Auslaender, Jiun-Haw Chu, James G. Analytis, Ian R. Fisher, and Kathryn A. Moler, “Local measurement of the superfluid density in the pnictide superconductor $\text{Ba}(\text{Fe}_{1-x}\text{Co}_x)_2\text{As}_2$ across the superconducting dome,” *Phys. Rev. Lett.* **106**, 067001 (2011).
- [22] R. T. Gordon, H. Kim, N. Salovich, R. W. Giannetta, R. M. Fernandes, V. G. Kogan, T. Prozorov, S. L. Bud’ko, P. C. Canfield, M. A. Tanatar, and R. Prozorov, “Doping evolution of the absolute value of the london penetration depth and superfluid density in single crystals of $\text{Ba}(\text{Fe}_{1-x}\text{Co}_x)_2\text{As}_2$,” *Phys. Rev. B* **82**, 054507 (2010).
- [23] Rustem Khasanov, William R. Meier, Yun Wu, Daixiang Mou, Sergey L. Bud’ko, Ilya Eremin, Hubertus Luetkens, Adam Kaminski, Paul C. Canfield, and Alex Amato, “In-plane magnetic penetration depth of superconducting $\text{CaKFe}_4\text{As}_4$,” *Phys. Rev. B* **97**, 140503 (2018).
- [24] DongHo Wu, W. L. Kennedy, C. Zahopoulos, and S. Sridhar, “Characteristics and growth of single crystals of $\text{YBa}_2\text{Cu}_3\text{O}_7$ with superior microwave properties,” *Appl. Phys. Lett.* **55**, 696–698 (1989).
- [25] J. L. Tallon, C. Bernhard, U. Binniger, A. Hofer, G. V. M. Williams, E. J. Ansaldo, J. I. Budnick, and Ch. Niedermayer, “In-plane anisotropy of the penetration depth due to superconductivity on the Cu-O chains in YBaCuO ,” *Phys. Rev. Lett.* **74**, 1008–1011 (1995).
- [26] J. E. Sonier, R. F. Kiefl, J. H. Brewer, D. A. Bonn, J. F. Carolan, K. H. Chow, P. Dosanjh, W. N. Hardy, Ruixing Liang, W. A. MacFarlane, P. Mendels, G. D. Morris, T. M. Riseman, and J. W. Schneider, “New muon-spin-rotation measurement of the temperature dependence of the magnetic penetration depth in $\text{YBaCuO}_{6.95}$,” *Phys. Rev. Lett.* **72**, 744–747 (1994).